Triacylglycerol structures and the chocolate fat bloom mechanism

van Mechelen, J.B.

Chapter 2

Structures of mono-unsaturated triacylglycerols

Part I

The β_1 polymorph

based on Acta Cryst. (2006) B**62**, 1121-1130

2.1 Abstract

The crystal structures of β_1 polymorphs of mono-unsaturated triacylglycerols have been solved from high-resolution laboratory and synchrotron powder diffraction data for five pure compounds, the 1,3-dimyristoyl-2-oleoylglycerol (β_1-MOM), 1,3-dipalmitoyl-2-oleoylglycerol (β_1-POP), 1,3-distearoyl-2-oleoylglycerol (β_1-SOS), 1-palmitoyl-2-oleoyl-3-stearoylglycerol (β_1-POS), 1-stearoyl-2-oleoyl-3-arachidoylglycerol (β_1-SOA) and three mixtures: the co-crystallized 1:1 molar mixture of SOS and POP (β_1-SOS/POP (1:1)) and two cocoa butters from Bahia and Ivory Coast, both in their β-VI (= β_1) polymorph. All eight β_1 structures are crystallized in space group $P2_1/n$ and have two short cell axes (5.44 - 5.46 Å and 8.18 – 8.22 Å) as well as a very long b axis (112 – 135 Å). The dominant-zone problem in the indexing of the powder patterns was solved with the special brute force indexing routine *LSQDETC* from the *POWSIM* program. Structures were solved using the direct-space parallel-tempering method *FOX* and refined with GSAS. Along the b axis, alternations of inversion-centre-related 'three-packs' can be discerned. Each 'three-pack' has a central oleic zone, with oleic acyl chains of the molecules being packed together, that is sandwiched between two saturated-chain zones. The conformation of the triacylglycerol molecules is relatively 'flat' because the least-squares plane through saturated chains also contains the saturated parts of the olein chain. The solution of the β_1 structures is a step forward towards understanding the mechanism of fat bloom formation in dark chocolate and has led to a reexamination of the β_2 structural model (Chapter 3; van Mechelen *et al.,*(2006)).

2.2 Introduction

Many consumer products contain fats in solid form. Fats, and their constituent triacylglycerols (TAGs), may crystallize in various solid-state phases (polymorphs) that have different melting points and stabilities. The main phases, the γ, α, β' and β, form a monotropic phase sequence ($\gamma \rightarrow \alpha \rightarrow \beta' \rightarrow \beta$) of increasing melting point and stability (van Malssen *et al*., 1999), although for some β' stable types of fats and TAGs the β phase does not crystallize. In general, during the production process a fat should be crystallized in its most stable phase to avoid phase transition(s) afterwards. For example, for cocoa butter, and the *cis* mono-unsaturated TAGs it consists of (Beckett, 1999), the β phase is the most stable, although this phase actually consists of two different β polymorphs, a lower melting β_2 phase, in case of cocoa butter being known as β-V, and a higher melting β_1 phase (in cocoa butter β-VI). The fat bloom problem of chocolate is commonly attributed to the phase transition β-V $\rightarrow$ β-VI (Wille & Lutton, 1966). In order to

understand this transition and other TAG phase transitions, structural models of the individual phases at the molecular level are required.

The ideal way to solve a crystal structure is using single-crystal X-ray diffraction data. For TAGs, however, this route has not been very successful because of the difficulty to grow large, good quality single crystals. Only structures of trisaturated TAGs have been obtained (Vand & Bell, 1951; Larsson, 1965; Jensen & Mabis, 1966; Doyne & Gordon, 1968; Gibon *et al*., 1984; Goto *et al*., 1992; van Langevelde *et al*., 1999; van Langevelde *et al*., 2000; Sato *et al*., 2001) and a tri-trans-mono-unsaturated structure (Culot *et al*., 2000). An alternative technique nowadays is to solve a crystal structure from powder diffraction data using direct-space search techniques. Helped by the existence of homologous, single-crystal-based crystal structures as start search models, several crystal structures of trisaturated TAGs were solved from synchrotron powder data (van Langevelde *et al*., 2000; van Langevelde *et al*., 2001; van Langevelde *et al*., 2002; Helmholdt *et al*., 2002). In recent years, the direct-space search techniques have been improved considerably and do not require single-crystal precursors anymore. This progress is essential for TAGs of the type SatOSat' (Fig. 2.1), with Sat and Sat' saturated acyl chains and O a mono-unsaturated oleoyl chain (C18:1 with a *cis* double bond) at the glycerol sn-2 position, for which single crystals are rare. The structure of β_2-SOS (S = stearoyl, C18:0) was the first to be obtained in this way, and to date it is still the sole published structural model of a mono-unsaturated TAG (Peschar *et al*., 2004).

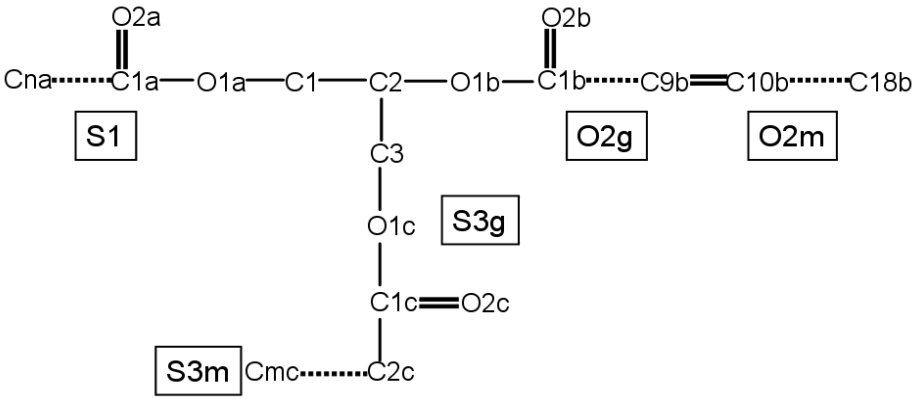

Fig. 2.1: Chemical structure diagram of SatOSat'-type TAGs. The numerical subscripts *m* and *n* (= 14, 16, 18, 20) label the acyl chain lengths while the S1, S3g, S3m, O2g and O2m label the saturated acyl chain and acyl-chain parts, respectively.

In this paper we present the crystal structures of eight β_1 phases, five of them being of pure TAGs: 1,3-dimyristoyl-2-oleoylglycerol (β_1-MOM), 1,3-dipalmitoyl-2-oleoylglycerol (β_1-POP), 1,3-distearoyl-2-oleoylglycerol (β_1-SOS), 1-palmitoyl-2-oleoyl-3-stearoylglycerol (β_1-POS) and 1-stearoyl-2-oleoyl-3-arachidoylglycerol (β_1-SOA). Furthermore, we obtained the β_1 polymorph structures of three mixtures of TAGs, a co-crystallized (1:1 M) mixture of SOS and POP (β_1-SOS/POP (1:1)) and the β-VI structures of cocoa butters from Bahia (β-VI Bahia) and Ivory Coast (β-VI Ivory Coast). The existence of the β_1 SOS/POP has not been reported before. The crystal structures have been solved from high-resolution synchrotron and laboratory powder diffraction data (HRPD). An analysis of the β_1 structures provides an explanation of the relative lower melting point (T_m) of the asymmetric TAGs compared to the symmetric ones and points out that the β_1 structures differ considerably from the published β_2-SOS polymorph.

2.3 Experimental Methods

2.3.1 Samples, sample preparation and data collection

All pure TAG samples were obtained from Unilever Research Laboratorium (Vlaardingen, The Netherlands). The cocoa butter samples were obtained from ADM (Koog a/d Zaan, The Netherlands). Both the pure TAGs (Schlenk, 1965) and the cocoa butter samples (Takagi & Ando, 1995) were racemic mixtures and have been checked for the presence of more than one polymorph on the in-house X'pertPro-alpha1 diffractometer (PANalytical, Almelo, The Netherlands) before carrying out the full data collection. All samples were put in glass capillaries that were spun during data collection. POP, SOS, POS and SOA were obtained as β_1 phase powders and required no further purification. With respect to POS and SOA, in the literature the highest-melting polymorph of POS is usually referred to as a β type, without further specification. (Arishima *et al*., 1991; Yano *et al.*, 1993). We have established that both these β polymorphs should be referred to as β_1 because of the existence of a lower-melting β_2 polymorph for both POS and SOA, which has not been previously reported in the literature. The crystal structures of β_2-POS and β_2-SOA will be reported in part II (H3; van Mechelen *et al*., 2006). β_1-MOM was recrystallized at 294 K from the melt by keeping it for several days at this temperature. A co-crystallized mixture of POP and SOS was prepared by melting a physical 1:1 molar mixture of POP and SOS and letting the melt recrystallize at 294 K. The β_1 polymorph was purified by a tempering

procedure (= cyclic heating and cooling) between 303 and 310 K. The cocoa butter samples were crystallized from the melt at 294 K. After several weeks the conversion of the Bahia sample into the β_1 polymorph was completed. The Ivory Coast cocoa butter sample was tempered between 302 and 307 K to purify the β_1 polymorph. All samples except Ivory Coast cocoa butter have been measured at the high-resolution powder diffraction station BM01b at the ESRF (European Synchrotron Radiation Facility, Grenoble, France). The Ivory Coast sample was measured in-house on the X'pert Pro-alpha1 diffractometer. This diffractometer was equipped with a sealed Cu X-ray tube, 0.01 rad primary and secondary Soller slits and a hybrid monochromator that produces a parallel Cu $K\alpha_1$ X-ray beam. The solid-state strip detector X'celerator (PANalytical) was used at its maximum active length of 2.17 °2θ. The data collection conditions for each of the samples are given in Tables 2.1 and 2.2. The continuous scans were binned with step sizes of 0.005 °2θ for the BM01b data and 0.008 °2θ for the X'pert Pro alpha1 data, respectively. Some of the samples appeared to have a small impurity line from unknown origin between the first and the second reflection. This peak has been excluded from the refinement (see Tables 2.1 and 2.2). Melting points have been determined with a DSC600 (Linkam Scientific Instruments Ltd, Tadworth, England) using a heating rate of 2 K min^{-1}. The melting points given in Tables 2.1 and 2.2 are the top of the melting peak. The DSC traces showed no evidence for the coexistence of more than one phase.

2.3.2 Indexing

A major problem to overcome before the actual structure determination of a TAG can be started is the indexing of its powder pattern. All TAG unit cells known to date have (at least) one small and one (very) long unit axis. If the ratio longest to shortest unit-cell axis exceeds ~ 10, the lower-angle part of the diffraction pattern becomes seriously dominated by a single reciprocal lattice zone. Also, the reflection density in the higher-angle part of the diffraction patterns causes serious peak-overlap problems and makes it difficult to obtain convincing indexing results. Therefore, it is no surprise that the generally used auto-indexing programs like *ITO*, *TREOR* and *DICVOL* cannot handle this problem. We used a different strategy and indexed the synchrotron powder patterns of β_1–SOS, β_1–POP, β_1–MOM, β_1–POS and β_1–SOA with the indexing routine *LSQDETC* that runs in conjunction with the program suite *POWSIM* (Peschar *et al.*, 2002). *LSQDETC* is a brute force program that searches systematically through the allowed solution space for cells. The solution space is defined by adjustable unit-

Table 2.1: Experimental and structural details of structure refinement of β_1 structures of symmetric molecules.

	β_1-MOM	β_1-POP	β_1-SOS-POP	β_1-SOS
Chem. form.	$C_{49}H_{92}O_6$	$C_{53}H_{100}O_6$	$C_{55}H_{108}O_6$	$C_{57}H_{108}O_6$
M_r	777.27	833.38	865.46	889.48
Cell setting	Monoclinic	Monoclinic	Monoclinic	Monoclinic
Space group	$P2_1/n$	$P2_1/n$	$P2_1/n$	$P2_1/n$
$T_{\text{data coll.}}$ (K)	295	295	295	295
a, b, c (Å)	5.453 (1)	5.450 (1)	5.447 (1)	5.442 (1)
	112.75 (1)	121.32 (1)	125.97 (1)	129.90 (1)
	8.195 (1)	8.209 (1)	8.212 (1)	8.184 (2)
β (°)	88.84 (1)	88.85 (1)	88.85 (1)	88.71 (1)
V (Å^3)	5038.0 (2)	5426.6 (5)	5633.7 (3)	5784.2 (5)
Z	4	4	4	4
D_x (Mg m^{-3})	1.025	1.020	1.020	1.021
T_m (K)	305.5	312	311	318
Radiation type	synchrotron	Synchrotron	synchrotron	Synchrotron
Specimen form, colour	Cylinder: solid fat, white	Cylinder : powder, white	Cylinder : solid fat, white	Cylinder: powder, white
Specimen size (mm)	2.5 × 1 × 1	20 × 1.5 × 1.5	4 × 1 × 1	20 × 1 × 1
Diffractometer	ESRF BM01b	ESRF BM01b	ESRF BM01b	ESRF BM01b
2θ range (°)	0.53 - 40.5	0.34 - 30.0	34, 2 - 40.5	0.53 - 30.0
R factors and goodness of fit	R_p = 0.068	R_p = 0.064	R_p = 0.051	R_p = 0.055
	R_{wp} = 0.098	R_{wp} = 0.086	R_{wp} = 0.063	R_{wp} = 0.068
	R_{exp} = 0.014	R_{exp} = 0.015	R_{exp} = 0.023	R_{exp} = 0.020
	S = 7.82	S = 6.02	S = 2.91	S = 3.66
λ(Å)	0.79936	0.79889	0.79889	0.75003
Excl. region(s)	No	No	0.85-0.965	0.738-0.897
No. of param.	489	516	547	550

cell parameter ranges and based on prior knowledge about the expected unit-cell volume windows and density of the material. To check the correctness of the indexing of the five patterns, the program *Chekcell* (Laugier & Bochu, 2001) was used. This latter program was also used iteratively to index the three patterns of TAG mixtures: β_1-SOS/POP (1:1), β-VI Bahia and β-VI Ivory Coast. Starting with the unit cell of β_1–SOS, the longest axis was modified manually until the calculated low-angle reflections matched the observed positions of diffraction maxima. After coupling the positions of the main peaks at higher angles to the proper peak positions of the current cell, the cell was refined after which the refined cell was taken as the new current cell. This procedure was repeated until a cell was found that explained all the diffraction maxima in the pattern.

Table 2.2: Experimental and structural details of structure refinement of β_1 structures of asymmetric molecules and β-VI cocoa butter.

	β_1-POS	β_1-SOA	β-VI Bahia	β-VI Ivory Coast
Chem. form.	$C_{55}H_{104}O_6$	$C_{59}H_{112}O_6$	$C_{54.96}H_{104}O_6$	$C_{55}H_{104}O_6$
M_r	861.43	917.54	860.90	861.38
Cell setting space group	Monoclinic $P2_1/n$	Monoclinic $P2_1/n$	Monoclinic $P2_1/n$	Monoclinic $P2_1/n$
$T_{\text{data coll.}}$ (K)	295	294	295	295
a, b, c (Å) β (°)	5.445 (1) 125.98 (2) 8.195 (1) 88.79 (1)	5.439 (1) 134.65 (1) 8.200 (1) 88.73 (1)	5.444 (1) 127.40 (1) 8.195 (1) 88.71 (2)	5.448 (1) 128.71 (1) 8.201 (2) 88.61 (1)
V (Å^3)	5620.3 (3)	6003.7 (4)	5682.8 (4)	5748.5 (1)
Z	4	4	4	4
D_x (Mg m^{-3})	1.018	1.015	0.997	1.000
T_{m} (K)	311.5	315	308	308.5
Radiation type	synchrotron	Synchrotron	synchrotron	Cu $K\alpha_1$
Specimen form, colour	Cylinder: powder, white	Cylinder: powder, white	Cylinder: solid fat, yellowish white	Cylinder: solid fat, yellowish white
Specimen size (mm)	5 × 1.5 × 1.5	5 × 1.5 × 1.5	20 × 1.5 × 1.5	12 × 1 × 1
Diffractometer	ESRF BM01b	ESRF BM01b	ESRF BM01b	X'pertPro-α1
2θ range (°)	0.53 - 48.2	0.51 - 53.3	0.53 - 43.0	0.79 - 50.0
R factors and goodness of fit λ(Å)	R_p = 0.062 R_{wp} = 0.071 R_{exp} = 0.028 S = 2.64 0.750033	R_p = 0.070 R_{wp} = 0.088 R_{exp} = 0.028 S = 3.45 0.85019	R_p = 0.046 R_{wp} = 0.059 R_{exp} = 0.015 S = 4.22 0.79936	R_p = 0.043 R_{wp} = 0.059 R_{exp} = 0.012 S = 5.09 1.54059
Excl. region(s)	No	0.738-0.897	0.83-1.125	No
No. of param.	532	551	554	552

2.3.3 Model building and analysis

In accordance with the published structure of β_2–SOS (Peschar *et al.*, 2004), a β_1–SOS starting model was constructed, consisting of two parallel stearoyl chains (S1, S3) and an oleoyl chain (O2) pointing in the opposite direction (Fig. 2.1). The oleoyl chain was split in two saturated partial chains, O2g (bonded to the glycerol) and O2m (methyl side) that are connected by a double bond at carbons C9b and C10b. During the refinement stage, also the S3 chain was split in two parts: S3g from C2 – C2c, *i.e.* from the glycerol group to the gauche band, and S3m from C2c to the end of the acyl chain. In relation to the models, the following geometrical parameters are used: the chain direction is defined as the least-squares line through a set of atoms, the chain plane is the least-squares plane through a set of C atoms and the molecule plane is defined as the least-squares plane through the directions of the chains S1, S3g, S3m, O2g and O2m.

The structure of β_1–SOS has been solved with the parallel tempering mode of the program *FOX* (Favre-Nicolin & Černý, 2002), using a *Z*-matrix description. In the initial stage of the structure-solution process only translation and rotation of the rigid starting model was allowed. Later, the torsion angles at the glycerol and at the C9b=C10b double bond were released one by one, starting at the latter. The saturated (parts of the) acyl chains were treated as rigid bodies. H atoms were included only in the final stage of the structure-solution process.

The final β_1–SOS model found by *FOX* was used as starting model for the other structures. Since MOM and POP are symmetric TAGs, just like SOS, the *Z* matrix of the latter can be edited and the S1 and S3 chain lengths can be shortened to obtain search models of MOM and POP. For each asymmetric TAG (SOA and POS), two models were built and refined, one having S1 and the other having S3 as longest chain.

Cocoa butter is a mixture of fats with POP, SOS and POS as main components (~ 75%). When these TAGs co-crystallize, an average crystal-structure results with partially occupied positions of C atoms at the end of the S1 and S3 chains. Analogous to the published β_2 structure, the β_1-SOS structure was used as starting model for the average cocoa butter β_1 structure. The occupancy of the last two C atoms of the S1 and S3 chains was fixed at 0.5. This is an estimated value as neither the exact composition of the cocoa butter is known nor what fraction of the main components co-crystallizes.

The co-crystallized mixture of SOS and POP (1:1 M) was also assumed to form an average crystal structure with POP and SOS distributed 1:1 over the molecule positions. The same starting model was used as for cocoa butter but now with a calculated occupancy of 0.5 for the last two C atoms of the S1 and S3 chains.

The structures were refined with *GSAS* (Larson & von Dreele, 1987) using a Chebyshev polynomial to fit the background and profile number 4 to describe the peak profiles. With this function low-angle peak asymmetry and *hkl*-dependent broadening could be modelled successfully. Soft restraints were applied to bonding angles and distances of all atoms, including the H atoms, to stabilize the refinement. The restraint values are mean values taken from the Cambridge Structural Database (CSD; Allen, 2002). The weight of the restraints applied to H atoms was taken half the weight applied to non-H atoms. Soft planar restraints were applied to the C atoms of the acyl chains S1, O2g, O2m and S3m, to the three C=O groups including the C atoms connected to them and to the C8b-C9b=C10b-C11b group. The weight of the restraints in the refinement process was reduced but its level was kept high enough to ensure a stable refinement. In the final stage of the refinement the contribution of the restraints to the total of the χ^2 residue parameter was ca 10%. The applied isothermal displacement parameters U_{iso} was 0.025 for non-H atoms and 0.05 for H atoms. Attempts to apply a coupled refinement of U_{iso} for all atoms did not result in a significant improvement of R values so the original U_{iso} values were retained. Preferred orientation was corrected for by the March–Dollase function (March, 1932; Dollase, 1986) for β_1-SOA (axis [010], ratio=1.06, correction range: Min=0.85, Max=1.09). For the other samples no significant PO was found. In §2.8 (appendix) the final results of the refinements are shown (Figs. 2.11-2.18).

2.4 Results and Discussion

2.4.1 Data collection

In Fig. 2.2 an overview is given of the diffraction patterns of all samples with the 2θ-values being converted to the same scale (2θ, Cu $K\alpha_1$ radiation). The low-angle parts of the diffraction patterns ($2\theta < 10°$) are dominated by ($0k0$) reflections and are quite similar, except for the peak positions. The fingerprint areas ($2\theta > 21°$) show larger differences (Fig. 2.3). The patterns of the two asymmetric molecules, the two cocoa butter samples and β_1-SOS/POP (1:1) have similar characteristics. The other three patterns of the symmetric molecules differ from each other and from the other five. The diffraction patterns suggest a similarity between the packing of the β_1-SOS/POP (1:1) and the asymmetric TAGs.

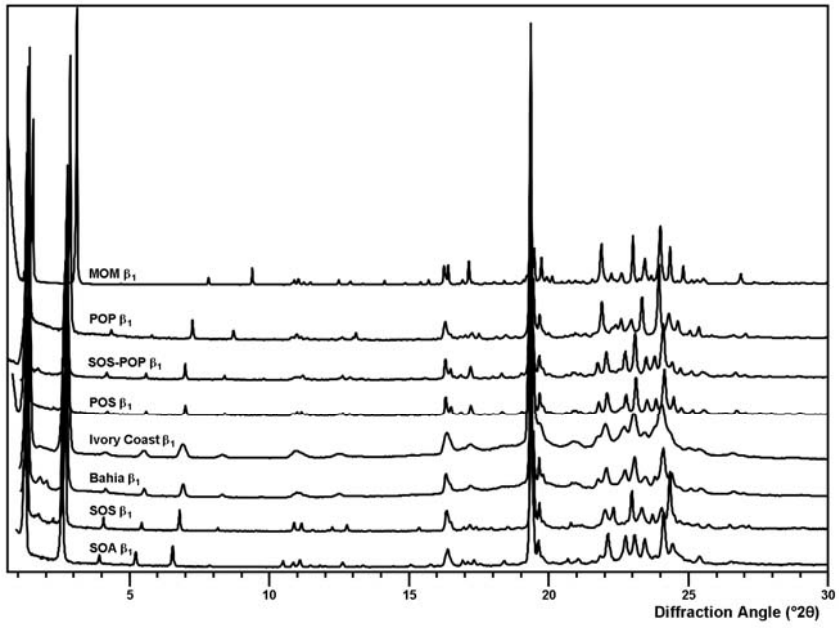

Fig. 2.2: Overview of β_1-diffraction patterns with 2θ scale converted to Cu $K\alpha_1$ radiation.

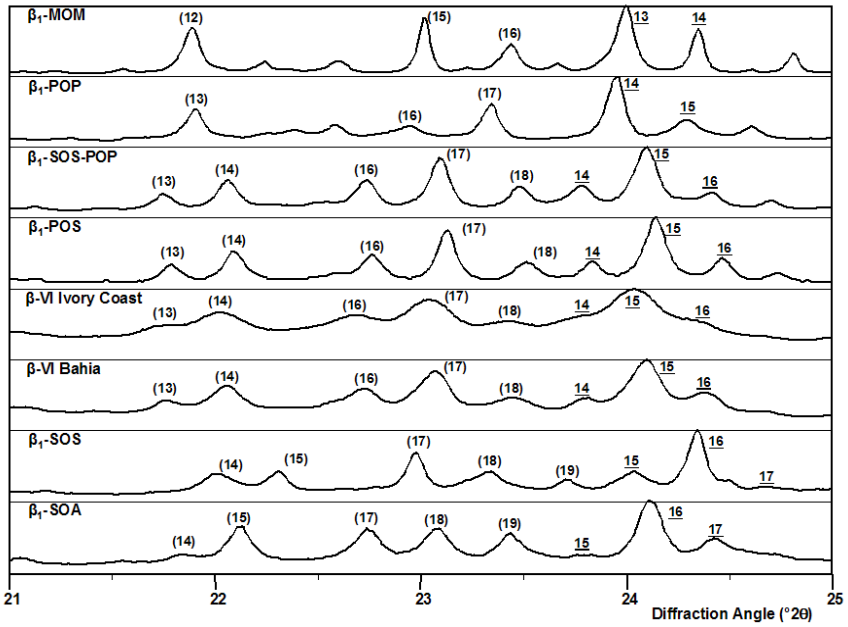

Fig. 2.3: Part of the higher angle area of Fig. 2.2 showing the differences between the patterns. $(1,k,\bar{1})$ peaks are labelled (k) and $(0,k,2)$ peaks are labelled $\underline{k}$.

2.4.2 Indexing, structure determination and refinement of the β_1 polymorphs

All eight patterns could be indexed on similar monoclinic cells (Tables 2.1 and 2.2) with $Z = 4$. The choice of space group, however, was not obvious because of the peak overlap. Assuming a single molecule in the asymmetric unit, the space group selection was limited to centrosymmetric space groups with a 4-fold general position. Systematic extinctions excluded the noncentrosymmetric space groups. From the centrosymmetric space groups six possibilities had to be tested: *P2/m*, $P2_1/m$, *P2/c*, $P2_1/c$, $P2_1/a$, and $P2_1/n$. This implied six structure determinations to be carried out in parallel. As this problem was the same for all the β_1 structures of this study, one of the patterns (β_1–SOS) was chosen to find the most probable space group. In the first three space groups no feasible structure solution could be found. The choice between the three settings of space group 14 ($P2_1/c$, $P2_1/a$, $P2_1/n$) was less obvious. At first glance all packings looked feasible but a closer look revealed an inferior packing of the O2 chain in $P2_1/a$ and $P2_1/c$ compared to a parallel side-by-side packing of the O2 chains in $P2_1/n$. Since in the structure-solution process also the *R* values appeared to be lower for $P2_1/n$, this space group was taken as the most probable one and this choice also turned out to hold for the other seven patterns as became clear during the refinement process.

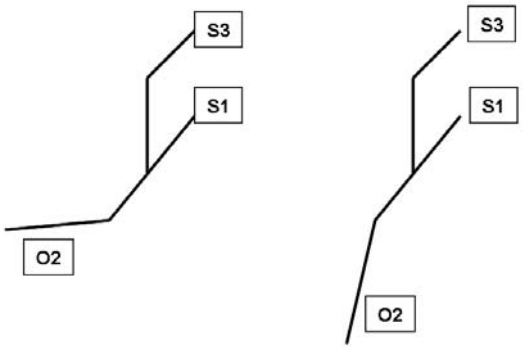

Fig. 2.4: TAG with flat (left) and rotated (right) conformation of the O2 chain.

During the structure-solution process, it appeared that the precise orientation of the direction of the O2m chain, compared to the direction of the S1, the S3 and the O2g chains, leads to two types of TAG packing, a 'flat' conformation and a 'rotated' conformation. In the former the direction of the O2m chain is in the same plane as the direction of the other three chains, whilst in the 'rotated' conformation the direction of the O2m is rotated out of this plane (Fig. 2.4). The different conformations imply different interconnections of the columns of electron density of the S1 and S3 chains to the glycerol (Fig. 2.5). It was not possible with *FOX* to discriminate between the two conformations. Only during structure refinement in *GSAS*, with *hkl*-dependent line broadening properly taken into account, it became clear that the refinement of the 'flat' conformation converged better.

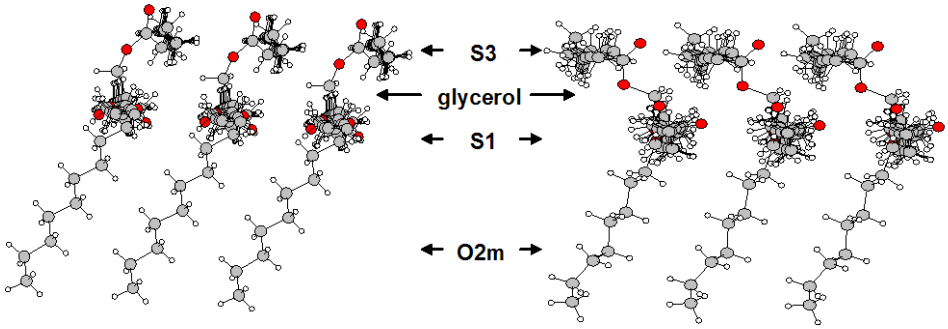

Fig. 2.5: Different orientation of glycerol in flat conformation (left) and rotated conformation (right). View parallel to the S1 and S3m direction.

Although in both the 'flat' and the 'rotated' conformation the zigzag acyl-chain planes S1, S3 and O2g are parallel, this parallelism is poorly defined as additional rigid-body refinement experiments pointed out. The S3m chain plane and the S1 chain plane were defined as rigid bodies in *GSAS* and rotated relative to each other using the (common) rigid-body axis direction as rotation axis. A rotation of 10° affected the *R* value somewhat but if this forced rotation was kept fixed during a subsequent structure refinement, its effect was almost completely compensated for by small changes in the structure. When the chains were rotated over 180° in this way in steps of 10° with subsequent refinement, the change in *R* value was less than 1% and the lowest *R* value did not always correspond to the 'flat' conformation starting point of the rotations. Apparently, this minimization involves a shallow *R* value valley and with some intervention a lower point in the valley may be found. Peak overlap facilitates the redistribution of intensities within

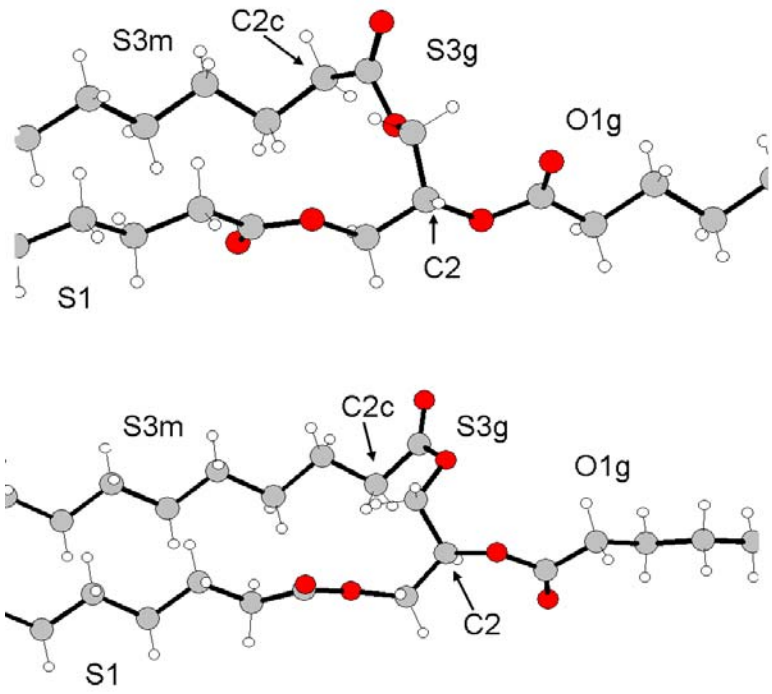

Fig. 2.6: The β_1-POS molecule conformation initially found by *FOX* (bottom) and the modified β_1-POS molecule conformation (top).

the envelope of the diffraction pattern after a forced rotation and limits the precision of, for example, the rotation angle of the zigzag planes around their longitudinal axis.

For the asymmetric TAGs, POS and SOA two models have been refined to find out whether S1 or S3 is the longest saturated chain. S3 appeared to be the longer chain as this resulted in the lowest *R* value.

The refinement of β_1-POS revealed that two different conformations are possible at the glycerol moiety with different S3g chain packings. In the β_1-POS model found by *FOX* (Fig. 2.6, bottom) and initially refined with *GSAS*, the S3g chain seems to be distorted and suffers from a C2 – C2c distance which is to short (3.29 Å). In an attempt to improve the conformation, both the S3m chain and the S1-O2 combination have been rotated around the longitudinal axis by 180° and the dihedral angles around the double bond in the middle of the O2 chain were modified to make the O2m chain point towards the original direction. After refinement of this new β_1-POS model (Fig. 2.6, top), the distance between C2 and C2c increased to 4.66 Å and the S3g chain remained almost flat. The *R* values of

both β_1-POS models did not differ significantly. The modified conformation has been applied to the other β_1 structures with the same effect: a nearly flat S3g chain and final R values that are equal to or slightly lower than those of the original models. Although the refinement is not decisive with respect to the correctness of the models, the flat conformation of the S3g chain is in line with published structures of β stable trisaturated TAGs (Jensen & Mabis, 1966; Gibon *et al*.,1984; van Langevelde *et al*., 1999; Culot *et al*., 2000; van Langevelde *et al*., 2001; van Langevelde *et al*., 2002; Helmholdt *et al*.,2002) and the β_1 molecule conformation as proposed by de Jong *et al.* (1991).

The assumed fractional occupancies of the two end atoms of the S1 and S3 chains in the SOS-POP (1:1) mixture and the cocoa butters did not change significantly as can be seen in the chemical formula of β-VI Bahia in Table 2.2, although this does not necessarily justify that these occupancies are correct as additional refinement experiments pointed out. A forced change of the occupancies with 0.05 mainly affects the intensities of the reflections (020) and (040) and when the structure is subsequently refined, while keeping the changed occupancies fixed, the changes are compensated for by small changes in the structure and virtually the same R value is obtained. Thus, the seemingly stable refinement of the occupancies of the two end atoms of the S1 and S3 chains is stable only because there is no driving force for a change. This implies that one should allow for a considerable error window on the partial occupancies.

For the SOS-POP (1:1) mixture two additional POS-like models were constructed and refined because SOS-POP (1:1) and POS have the same P:S ratio of 1 and their T_m and b-axis lengths are quite similar (Tables 2.1 and 2.2). The two asymmetric POS-like models were constructed from the final structure of the symmetric SOS model (the two last C atoms of S1 and S3 having an occupancy of 0.5) in the following way: (i) model A via a change of the fractional occupancies of the S1 end atoms to 0 and those of S3 to 1, (ii) model B by changing the fractional occupancies of the S1 end atoms to 1 and those of S3 to 0. The final R_p for the symmetric model was 0.0505, for the asymmetric model A 0.0544 and for asymmetric model B 0.0579. These R_p values suggest the symmetric model to be the most likely one, although also an asymmetric model can be argued for, as discussed below in § 2.4.5.

2.4.3 Influence of data resolution

The above-sketched problems to find the most probable conformation of the molecule can be attributed mainly to the limited crystallinity of the materials and their anomalous packing habit. The small and anisotropic crystallite sizes and the size of the unit cell cause *hkl*-dependent peak broadening and severe overlap in

the fingerprint area and, even when using high-resolution synchrotron radiation, the materials do not diffract significantly beyond the fingerprint area (*d* spacings 3 - 6 Å). As a result, atomic resolution was not obtained in any case. In most cases the data were collected up to atomic resolution and it may be argued that these data should be included in the refinement, in spite of lacking significant diffraction signal. After having carried out several refinement tests, the results refute this hypothesis. For example, β_1-POS was refined initially with diffraction data from 0.53 – 20 °2θ. The angle range was later extended by 10° to bring it in line with those of the other samples and to test the influence of these higher-angle data that lack significant diffraction signal. The extension hardly affected the refined crystal structure and the sole effect was a reduction of the *R* values: R_p from 0.0668 to 0.0616, R_{wp} from 0.0821 to 0.0706 and GOF from 2.95 to 2.64%. Thus, inclusion of high-angle diffraction data without any significant peak information does not necessarily have a positive influence on the structure refinement, as may be suggested by the lower *R* values.

2.4.4 The β_1 polymorph crystal-structure models

Fig. 2.7 shows the conformation of β_1-SOS and β_1-SOA, which are representative of symmetric and asymmetric β_1-SatOSat'-type TAGs, respectively. The molecules have the expected tuning fork conformation (Larsson, 1972; de Jong, *et al.,* 1991; Sato & Ueno, 2001). The least-squares lines through the different chains are approximately in the same plane, making the molecular conformation flat. The directions of the S1 and O2g chains are in line with each other. The orientations of the planes of all the chains are perpendicular to the plane of the molecule. The conformation of the symmetric and asymmetric molecules is the same and agrees well with the model of β_1-SOS proposed in literature (de Jong, *et al.,* 1991; Sato & Ueno, 2001). In going from POP to POS or from SOS to SOA the elongation of the S3 chain is realized by just adding two C atoms resulting in a slightly longer *b* axis.

When viewed along the two short axes, the packing of the TAGs consists of a sequence of six acyl-chain layers or, more precisely, of two sets of tri-acyl chain layers, from now on referred to as 'three-packs', which are symmetry related by inversion centres. Each 'three-pack' consists of an unsaturated zone, in which O2 chains are packed parallel and side-by-side, *i.e.* sandwiched by zones (Fig. 2.8). Interestingly, Filer *et al.* (1946) already proposed the existence of a six acyl-chain packing with saturated and unsaturated chain zones and de Jong *et al.* (1991) even argued $P2_1/a$ to be a good candidate space group. The unsaturated bond geometry is of the type *skew-cis-skew'*. The C9b=C10b double bonds of the O2 chains are

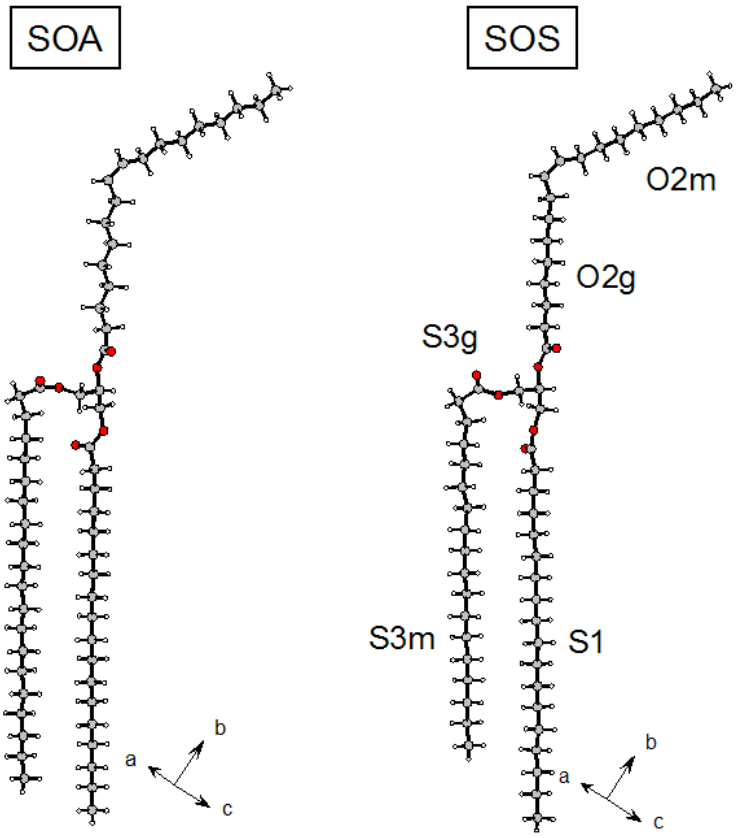

Fig. 2.7: Conformation of β_1-SOA and β_1-SOS molecules.

aligned at distances of 4.5 – 5.0 Å, thus too large for an olefinic π-π interaction. The acyl-chain layers are parallel to the *a* axis, *i.e.* perpendicular to the plane of drawing in Figs. 2.8(a) and 2.8(b) and largely parallel to the lattice plane (0*k*2) (Fig. 2.9) that corresponds to the strongest peak in the interval 23.9 - 24.5 °2θ (Fig. 2.3). The *k* index of this lattice plane varies with the length of the *b* axis. In a view parallel to the (10$\bar{1}$) (Fig. 2.8c), the acyl zigzags are largely parallel to the (1*k*$\bar{1}$), visible as the strongest peak in the interval 22.9 - 23.5 °2θ (Fig. 2.3) with the *k*-index again depending on the length of the *b* axis. A view parallel to (101) (Fig. 2.8d) emphasizes that the molecule planes are largely parallel to this lattice plane. The (111) (not shown) is slightly tilted relative to the (101) plane and intersects the molecule planes. The (111) and the (101) greatly overlap and form the strongest fingerprint diffraction maximum (Fig. 2.2, 19.4 °2θ, Cu $K\alpha_1$). The intensity of this peak is dominated by the (111) plane.

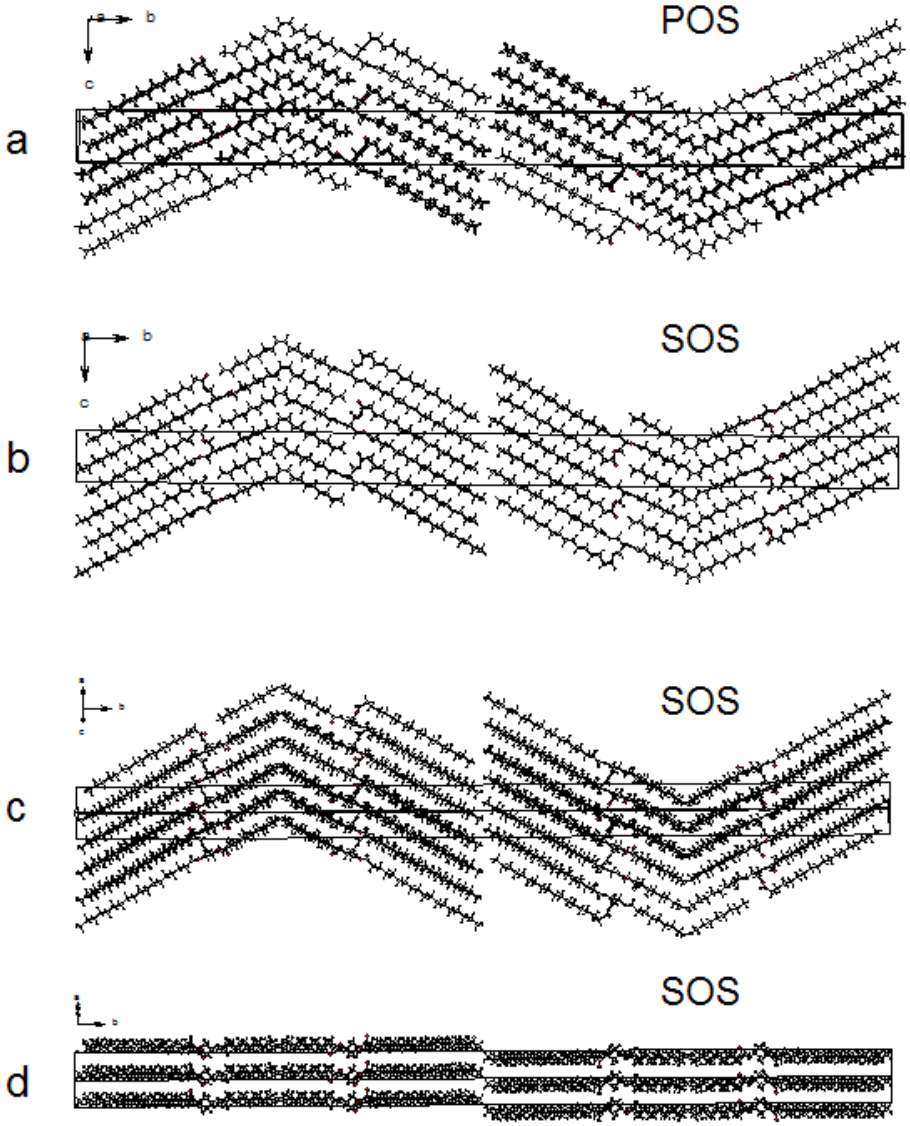

Fig. 2.8: Views down the a axis of (a) β_1-POS and (b) β_1-SOS. Views parallel to the $(10\bar{1})$ and (101) of β_1-SOS (c) and (d), respectively.

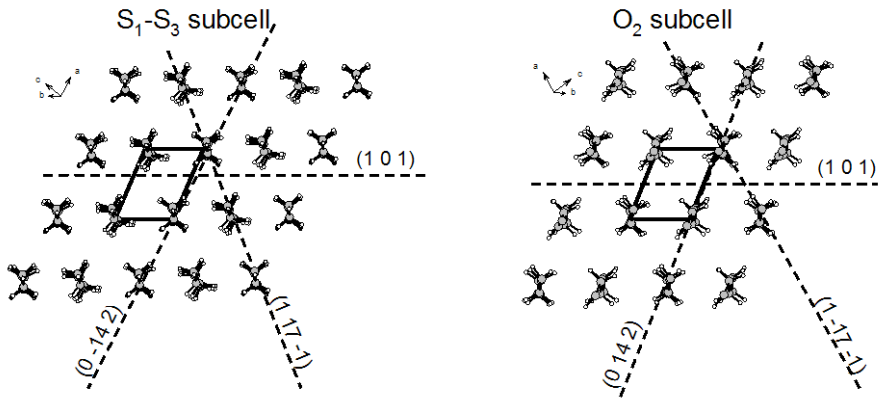

Fig. 2.9: The $M_{\parallel}$ subcells formed by saturated and by the oleoyl chains of β_1-POP with lattice plane markers.

With respect to the subcell and using the notation of Abrahamsson *et al.* (1978) the S1 and S3 chains together form a $M_{\parallel}$ subcell, while the O2 chains form a (different) $M_{\parallel}$ subcell (Fig. 2.9). A parallel chain packing has also been inferred from FT-IR measurements (Yano e*t al.*, 1993) but monoclinic subcells contradict the usual assumptions, $T_{\parallel}$ for the S-chains and $T_{\parallel}$ or $O'_{\parallel}$ for the O2 chains (Larsson, 1972; Yano e*t al.*, 1993).

Molecules of adjacent layers, and thus also the S1 and S3 chain planes of adjacent layers, are not aligned. The methyl end-plane is not flat but terrace-like (Figs. 2.8a and b). The terraces shown are not on the same level, as is suggested by the projection, but shifted relative to each other perpendicular to the plane of the molecules. The terraces in the symmetric MOM, POP and SOS are formed by the S1 and S3 chains of the same molecule, whereas in POS and SOA the terraces are formed by chains of different molecules. This difference in terrace is the consequence of the longer S3 chain in the asymmetric molecules. The co-crystallized samples have the same terrace position as the symmetric molecules as their conformation is based on the SOS model. The shortest chain distances between the 'three-packs' at the methyl end-plane range from 3.8 to 5.1 Å for the samples in this study. In these values the partial occupancy of the end atoms of the S1 and S3 chains has been taken into account by omitting two C atoms at one side of the distance. No clear relation seems to exist between chain lengths and molecular (a-)symmetry.

In view of the resolution of the data, a detailed analysis of the glycerol torsion angles has not been carried out.

2.4.5 The relation between melting point and methyl end-plane packing

The melting point T_m is a function of the chain length but also of the interaction between methyl groups at the methyl end-plane. The melting points of the symmetric MOM, POP and SOS show a linear relation (Fig. 2.10). As the methyl end-planes are equal, this relation reflects the difference in chain length. It is likely that the co-crystallized cocoa butter samples have a partially occupied methyl end-plane, because of the presence of TAGs with different saturated acyl-chain lengths. The partial occupation results in a T_m below the line through the symmetric T_ms. The T_ms of the asymmetric POS and SOA are also below this line but their crystal structures provide no evidence for any partial occupation at the methyl end-planes and they differ from the symmetric TAGs only in the position of the terraces at the methyl end-planes. De Jong *et al.* (1991) calculated lattice energies for single layers of symmetric and asymmetric monounsaturated TAGs and concluded that the addition of two C atoms essentially does not change the terrace structure of the methyl interface, but that for entropy reasons the T_m level is 4 K beneath that of the symmetric samples. Arishima *et al.* (1991) suggested the lowered T_m for POS to be due to racemic problems. Since all compounds in our study are racemic mixtures, it seems unlikely that only the asymmetric ones would show such problems. Schlenk (1965) crystallized racemic POS as well as the antipodes and found the former to yield β crystals while the pure enantiomers crystallize in the β' form but not in the β form. A comparison of the structures provides an alternative explanation. The difference in the length of the b axis between MOM and POP is 8.61 Å and between POP and SOS 8.59 Å, so an

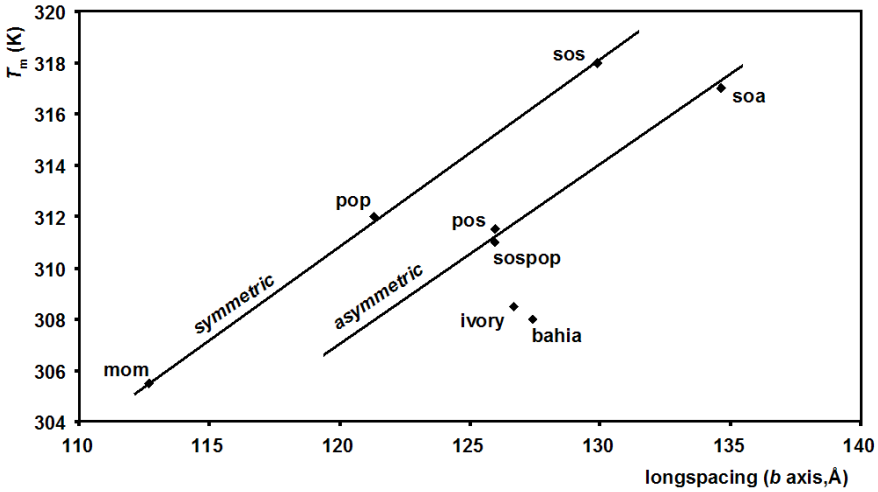

Fig. 2.10: Melting point (T_m) in relation to the long spacing. T_m(asymmetric) is 4 K below T_m(symmetric).

extension of both the saturated chains with two C atoms increases the *b* axis on average 8.6 Å. Between the asymmetric POS and SOA and the nearest symmetric molecules there is only one saturated chain that differs two C atoms in length and a *b* axis difference of 4.3 Å would have been in line with the behaviour of the symmetric molecules. The real difference between the *b* axis of POP and POS is 4.66 Å and between SOS and SOA 4.75 Å. Thus, the *b* axis of the asymmetric molecules is larger than may be expected on the basis of the behaviour of the symmetric molecules. The SOS-POP (1:1) crystal structure contains two different symmetric molecules but behaves like the asymmetric POS with an equal average chain length, equal *b* axis and an almost equal T_m. The larger *b* axis suggests a weaker interaction at the methyl interface and a corresponding lower melting point. Because of this similarity, an asymmetric model for SOS-POP (1:1) seems more likely than a symmetric one, in spite of the slightly lower R_p value. If this hypothesis is correct, the difference in terrace (location) seems to be a key factor in explaining the lower melting points of the asymmetric compounds. Unfortunately, the resolution of all data is not sufficient to draw this conclusion.

The Ivory Coast sample was more difficult to crystallize in the β_1 form than the Bahia sample, probably because of their compositional difference, the most prominent being Bahia's 10% higher content of TAGs with 2 oleic chains (van Malssen *et al.,* 1996). However, no significant difference could be established between the β_1 crystal structures of the two cocoa butter samples within the resolution of the HRPD data. The small differences in T_m and long spacing (*b* axis) also suggest that the average β_1 crystal structures differ only slightly in composition.

2.5 Conclusions

The β_1 polymorphs of Sat-O-Sat' type TAGs and the equivalent β-VI form of cocoa butter point out that high-resolution powder data can be sufficient for a successful crystal-structure determination, even if the data are not of atomic resolution. Based on the structure models and data, we were able to answer long-standing questions about the precise packing of the β_1 polymorphs, to interpret the characteristic fingerprint area in terms of the type of reflections involved and to rationalize the difference in melting points between symmetric and asymmetric TAGs.

Finally, the β_1 models led us to re-analyze the published β_2 model and the data it is based upon, the results of which will be presented in Chapter 3 (van Mechelen *et al*., 2006).

2.6 Acknowledgements

The authors thank ADM Cocoa NL for providing the cocoa butter samples and Unilever Research Vlaardingen and Unilever Research Colworth for the pure triacylglycerols. The authors acknowledge the ESRF (Grenoble, France) for providing the facilities to perform the synchrotron diffraction experiments and they thank the staff of the Swiss-Norwegian CRG beamline BM01b, D. Testemale, H. Emerich and W. van Beek, for their valuable help during the experimental sessions. The authors also thank K. Goubitz, E. Sonneveld, R.B. Helmholdt, M.M. Pop and D. J.A. De Ridder (all UvA) for their help in data collection during various experimental sessions at BM01b. Dr. V. Favre-Nicolin (INAC, Grenoble) is gratefully acknowledged to implement requested modifications in *FOX*. The investigations have been supported by the Netherlands Foundation for Chemical Research (NWO/CW) with financial aid from the Netherlands Technology Foundation (STW) (project 790.35.405). The members of the User Committee of this project are thanked for stimulating discussions and continuous interest.

2.7 References

Abrahamsson, S., Dahlén, B., Löfgren, H. & Pascher, I. (1978). *Prog. Chem. Fats other Lipids* **16**, 125-143.

Allen, F.H. (2002). *Acta Cryst.* B**58**, 380-388.

Arishima, T., Sagi, N., Mori, H. & Sato, K. (1991). *J. Am. Oil Chem. Soc.* **68**, 710-715.

Beckett, S.T. (editor) (1999). *Industrial chocolate manufacture and use*. Oxford: Blackwell Science.

Culot, C., Norberg, B., Evrard, G. & Durant, F. (2000). *Acta Cryst.* B**56**, 317-321.

De Jong, S., van Soest, T.C. & van Schaick, M.A. (1991). *J. Am. Oil Chem. Soc.* **68**, 371-378.

Dollase, W.A. (1986). *J. Appl. Cryst*. **19**, 267-272.

Doyne, Th.H., & Gordon, J.T. (1968). *J. Am. Oil Chem. Soc.* **45**, 333-334.

Favre-Nicolin, V. & Černý, R. (2002). *J. Appl. Cryst*. **35**, 734-743.

Filer, L.J. Jr., Sidhu, S.S., Daubert, B.F. & Longenecker, H.E. (1946). *J. of Am. Chem. Soc.* **68**, 167-171.

Gibon, V.; Blanpain, P.; Norberg, B. & Durant, F. (1984). *Bull.Soc. Chim. Belg*. **93**, 27-34.

Goto, M. Kodali, D.R., Small, D.M., Honda, K., Kozawa, K. & Uchida, T. (1992). *Proc. Natl. Acad. Sci. USA* **89**, 8083-8086.

Helmholdt,R.B.; Peschar,R.; Schenk,H. (2002). *Acta Cryst.* B**58**, 134-139.

Jensen, L.H. & Mabis, A.J. (1966). *Acta Cryst.* **21**, 770-781.

Langevelde, A. van, van Malssen, K., Hollander, F., Peschar, R. & Schenk, H. (1999). *Acta Cryst.* B**55**, 114-122.

Langevelde, A. van, van Malssen, K.F.; Driessen, R., Goubitz, K., Hollander, F.F.A.; Peschar, R., Zwart, P., Schenk, H. (2000). *Acta Cryst.* B**56**, 1103-1111.

Langevelde, A. van, Peschar, R. & Schenk, H. (2001). *Acta Cryst.* B**57**, 372-377.

Langevelde, A. van, Peschar, R. & Schenk, H. (2002). *Chem. Mater.* **13**, 1089-1094.

Larsson, K. (1965). *Arkiv Kemi* **23(1)**, 1-15.

Larsson, K. (1972). *Fette Seifen Anstrichm.* **74**, 136-142.

Larson, A.C. & Von Dreele, R.B. (1987). *GSAS, General Structure Analysis System*, Los Alamos National Laboratory: Report No. LA-UR-86-748.

Laugier, J. & Bochu, B. (2001). *Chekcell*, http//www.inpg.fr/LMPG.

March, A. (1932). *Z. Kristallogr*. **81**, 285-297.

Malssen, K.F. van, Peschar, R. & Schenk, H. (1996). *J. Am. Oil. Chem. Soc*. **73**, 1217-1223.

Malssen, K.F. van; van Langevelde, A.J.;Peschar, R. & Schenk, H. (1999) . *J. Am. Oil Chem. Soc*. **76**, 669-676.

Mechelen, J.B. van, Peschar, R. & Schenk, H. (2006). *Acta Cryst.* B**62**, 1131-1138.

Peschar, R., Etz, A., Jansen, J. & Schenk, H. (2002). *Structure determination from powder diffraction data*, edited by W.I.F. David, K. Shankland, L.B. McCusker & Ch. Baerlocher, Chapter 10. Oxford: Oxford Univ.Press.

Peschar, R., Pop, M.M., De Ridder, D.J.A., van Mechelen, J.B., Driessen, R.A.J. & Schenk, H. (2004). *J. Phys. Chem. B* **108**, 15450-15453.

Sato, K., Goto, M., Yano, J., Honda, K., Kodali, D.R. & Small, D.M. (2001). *J. Lipid Res*. **42**, 338-345.

Sato, K. & Ueno, S. (2001). *Crystallization processes in fats and lipid systems*, edited by N. Garti, & K. Sato. ,Chapter 5. New York: Marcel Dekker .

Schlenk, W. Jr. (1965). *J. Am. Oil. Chem. Soc.* **42**, 945-957.

Takagi, T. & Ando, Y. (1995). *J. Am. Oil Chem. Soc*. **72,** 1203-1206.

Wille, R.L. & Lutton, E.S. (1966). *J. Am. Oil Chem. Soc*. **43**, 491-496.

Yano, J., Ueno, S., Sato, K., Arishima, T., Sagi, N., Kaneko ,F. & Kobayashi, M. (1993). *J. Phys. Chem.* **97**, 12967-12973.

2.8 Appendix

Rietveld refinement results of β_1-structures

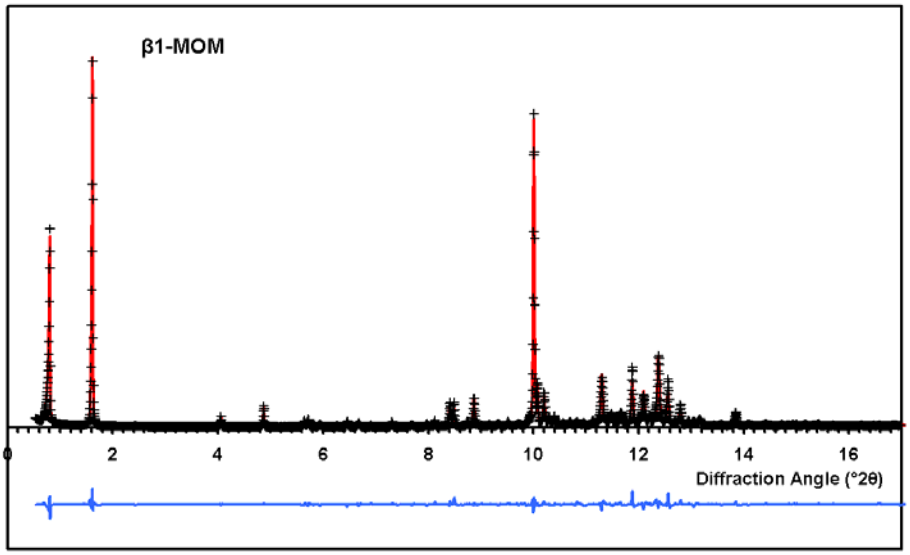

Fig. 2.11: Rietveld refinement results: Observed (+), calculated (solid) and difference (observed-calculated, lower curve) diffraction patterns of the refined β_1-structure of MOM.

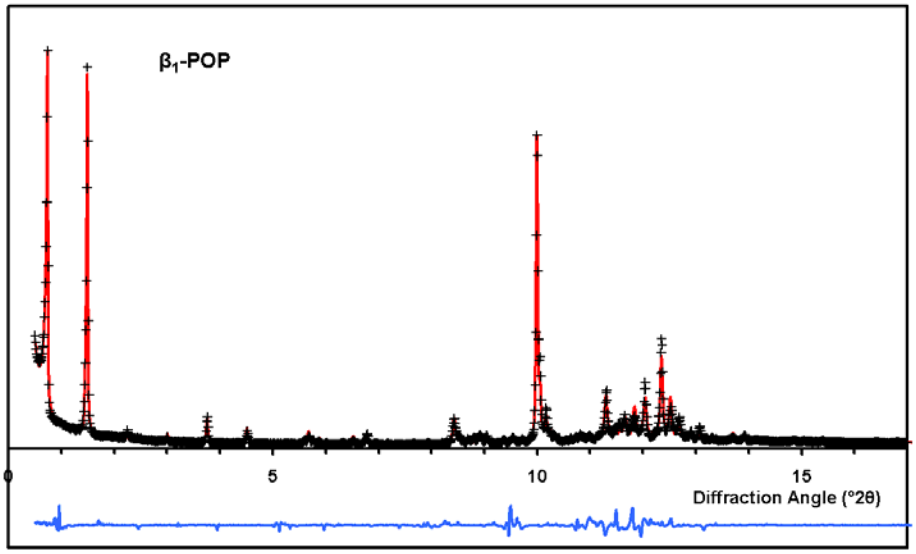

Fig. 2.12: Rietveld refinement results: Observed (+), calculated (solid) and difference (observed-calculated, lower curve) diffraction patterns of the refined β_1-structure of POP.

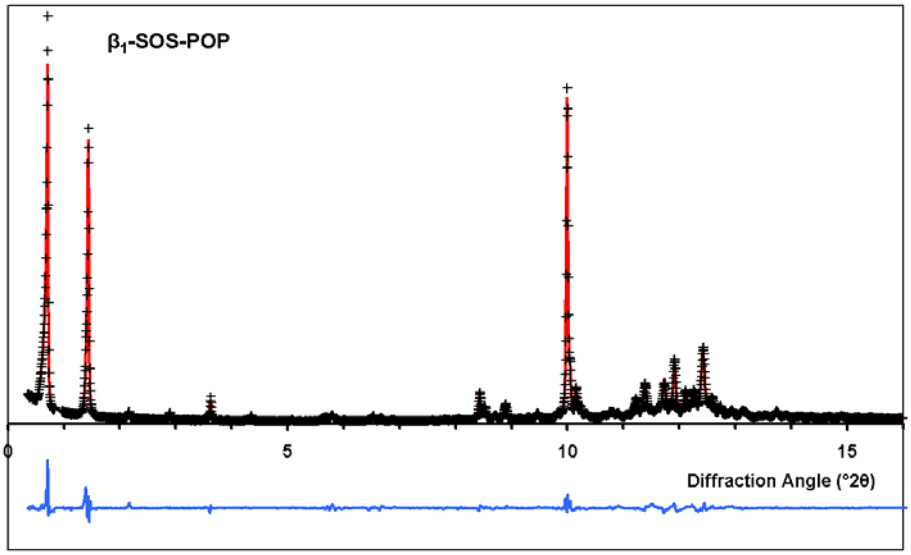

Fig. 2.13: Rietveld refinement results: Observed (+), calculated (solid) and difference (observed-calculated, lower curve) diffraction patterns of the refined β_1-structure of SOS-POP.

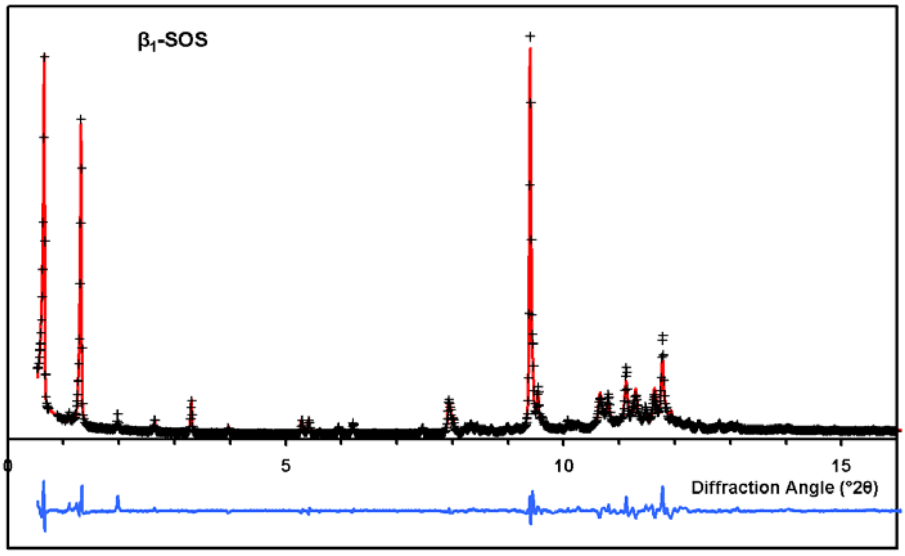

Fig. 2.14: Rietveld refinement results: Observed (+), calculated (solid) and difference (observed-calculated, lower curve) diffraction patterns of the refined β_1-structure of SOS.

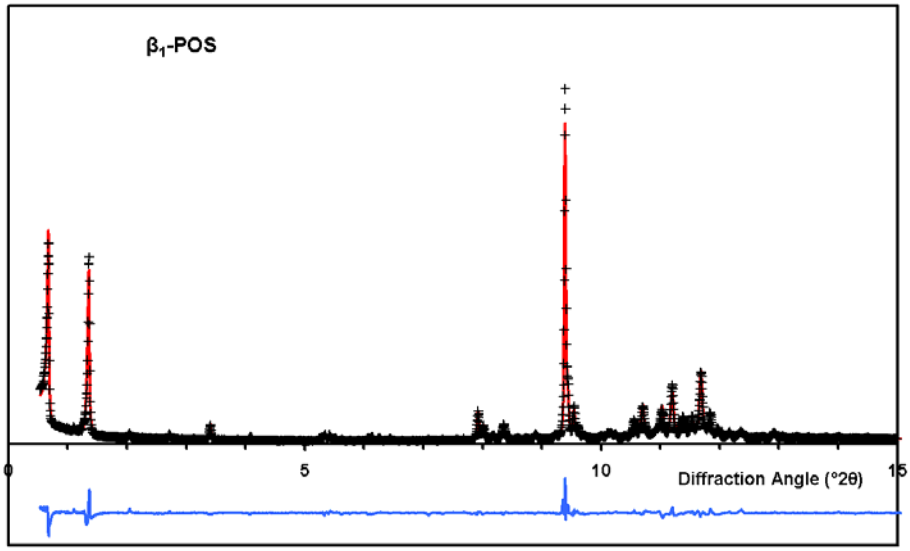

Fig. 2.15: Rietveld refinement results: Observed (+), calculated (solid) and difference (observed-calculated, lower curve) diffraction patterns of the refined β_1-structure of POS.

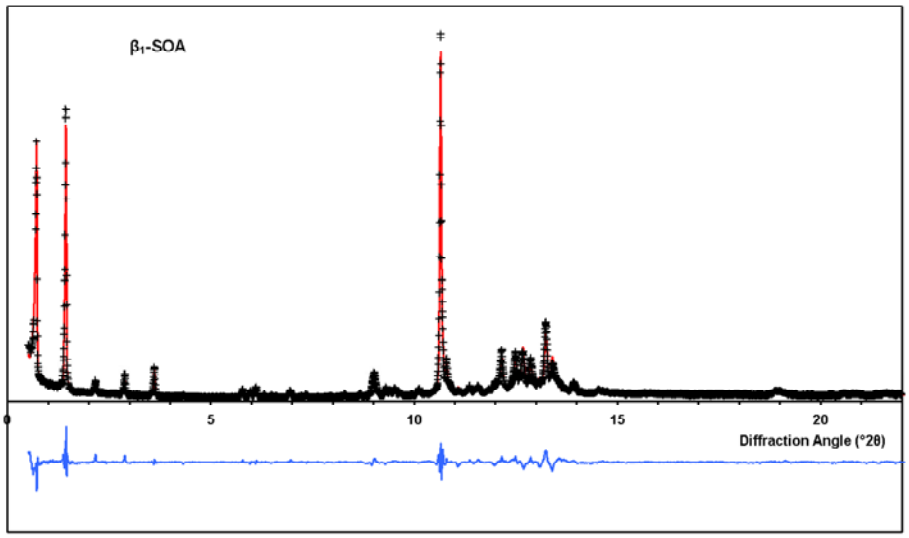

Fig. 2.16: Rietveld refinement results: Observed (+), calculated (solid) and difference (observed-calculated, lower curve) diffraction patterns of the refined β_1-structure of SOA.

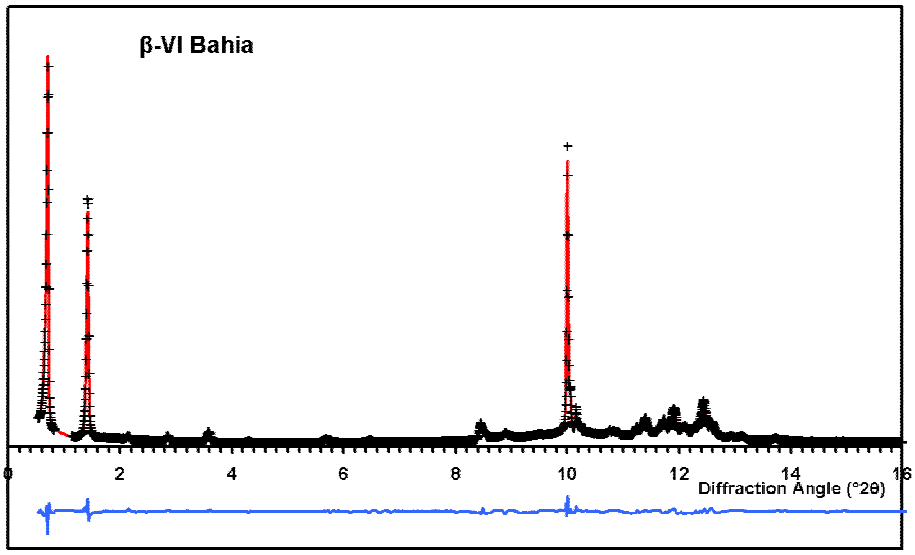

Fig. 2.17: Rietveld refinement results: Observed (+), calculated (solid) and difference (observed- calculated, lower curve) diffraction patterns of the refined β-VI-structure of Bahia cocoa butter.

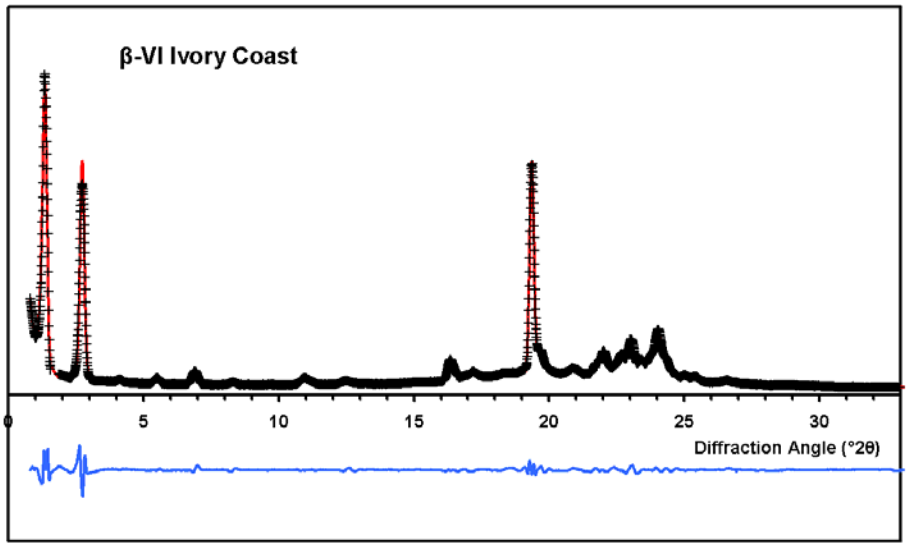

Fig. 2.18: Rietveld refinement results: Observed (+), calculated (solid) and difference (observed-calculated, lower curve) diffraction patterns of the refined β-VI structure of Ivory Coast cocoa butter.